QUARTERLY PROGRESS REPORT

prepared by

AVCO EVERETT RESEARCH LABORATORY
a division of
AVCO CORPORATION
Everett, Massachusetts

Contract NAS8-20310

July 1967

prepared for

HEADQUARTERS
NATIONAL AERONAUTICS AND SPACE ADMINISTRATION
OFFICE OF ADVANCED RESEARCH AND TECHNOLOGY
Washington, D. C.

TABLE OF CONTENTS

I. Introduction

This report covers progress made under Contract NAS8-20310 in the period 24 March 1967 to 23 June 1967. The relationship of the Technical work reported here and work performed under Contract AF49 638)-1553 continues to be as indicated in previous Quarterly Progress Reports.

During the present quarter progress has been made in several directions. In the experiment, voltages in excess of 200 kv have been achieved. These voltages were inferred using total charge measurements. It has been found that the total charge in the torus can be accurately measured by using the current buttons to measure the frequency of the fundamental diocotron oscillation (small amplitude). Because of the usefulness of this diagnostic, considerable theoretical effort has again been directed towards the study of diocotron waves. Most notably, it has been found that the only measurable small amplitude $\ell = 1$ diocotron mode has a frequency given only by the magnitude of the total charge and the magnetic field, independent of the charge distribution. Non-linear solutions have been exhibited, and the behavior of a diocotron wave during cloud compression has been studied.

Considerable experimental effort has also been directed towards a detailed study of the limits occurring during charge injection. From these studies it is believed that the current now injected is about as large as possible within the geometrical constraints of the present apparatus. However, we have found a strong correlation showing that we are injecting current only during a time window between Hull cutoff and the occurance of anamolous beam noise. The correlation with the occurance of anamolous noise indicates that we shall have to program the filament voltage $V_{fil} \propto B^2$.

Initial experimental and theoretical work has been started on the design of an experiment to check the feasibility of new shapes for a Plasma Radiation Shield.

Finally, a number of papers are in varying stages of publication and several oral presentations have been made at relevant technical conferences.

II. Spacecraft Integration and Other Related Considerations

In the area of spacecraft integration a milestone was reached with the publication of the report "The Plasma Radiation Shield: Concept, and Applications to Space Vehicles." This report was distributed with the March 1967 Quarterly Progress Report. An effort has been made to distribute this report as widely as possible among the people with an interest in the radiation shielding problem, and to follow this up where possible with personal contacts. Preliminary reactions to the report indicate a generally favorable reception. In particular, the new configuration (Fig. 3.4) appears to show considerable promise. In addition, the observation (especially Fig. 4.1) that modest voltages can produce substantial decrements in shielding techniques is a very strong point.

In order to achieve still wider distribution of this paper we have been preparing a shortened version for publication in the Journal of Spacecraft and Rockets which should reach a very large number of engineers. This new version is presently nearly finished.

III. Solenoidal Experiment

An experiment is being planned to explore the possibilities of constructing plasma radiation shields with a more cylindrical shape than considered in the past. The scaling of such an experiment is being examined with respect to the acceptable length and diameter of the solenoidal coil which would be used to produce the magnetic field. The limiting criteria being used for determining the shape and strength of the magnetic field is that the field lines containing electrons shall not pass too close to the walls of the available three-foot diameter vacuum tank and the magnetic field should be strong enough to contain a "reasonable" electron density, i.e., a density sufficient to produce a measurable space charge potential of at least several hundred volts.

A stainless steel vacuum tank about three feet in diameter is available for this experiment. This tank is capable of vacuums of the order of 10^{-7} torr.

It may be necessary to make the solenoid coil superconducting. Preliminary calculations indicate that a modest superconducting coil 2 inches in diameter should easily contain a 20-inch diameter electron cloud at a space charge potential of several hundred volts.

It is expected that this experiment will be assembled during the next quarter.

IV. Calculations Referring to the Solenoidal Experiment

A computational effort has been started with the object of finding equilibrium distributions for the electrons around a Plasma Radiation Shield of solenoidal shape. This calculation starts from the assumption of a given axially symmetric magnetic field geometry and a given quantity of electrons on each flux surface. The object of the calculation is to see how the electrons spread themselves out along the field lines in equilibrium.

While a number of possible methods of approaching this problem have been considered, we are presently proceeding along the following lines: each flux tube is broken up into a number of cells in the direction of the magnetic field. These cells are really hoops surrounding the axis of symmetry; the cross section of each of these hoops is roughly square, two sides being parallel to the magnetic field lines and two sides perpendicular. With each of these cells is associated a certain quantity of charge. The potential at the center of any cell due to a unit charge occupying any other cell is calculated. The total electrostatic energy is then a bilinear form in the amount of charge occupying each cell. In equilibrium this electrostatic energy must be a minimum and we therefore seek to minimize the energy subject to the following constraints:

1. Since charge is supposed free to move along field lines but not across, the sum of the charges in any flux tube is a given constant. This constraint is linear.

2. A non-linear constraint arises due to the fact that each charge must be negative or zero, i.e., we have only electrons. In the absence of this constraint unrealistic results will in general be found.

A program to perform minimization under constraints of this type has been found and is presently in use. Some running has already been done, but the results so far, while encouraging, are not yet completely satisfactory. The point of difficulty seems to be a correct evaluation of the self energy associated with each charge.

It is expected that this program will be completed during the coming quarter.

V. Diocotron Theory

Three advances of importance in diocotron theory have been made. These are: a) exhibition of exact large amplitude (non-linear) motions, having the character of diocotron waves; b) detailed solutions for small amplitude disturbances in a case of current experimental interest, and c) behavior of the diocotron wave when the magnetic field is slowly changed. All these topics deal with the basic geometry shown in Fig. V-1; an infinite conducting cylinder of radius a contains a uniform magnetic field B in the z-direction, and an electron cloud whose density is so low that $q = \omega_p^2/\omega_c^2 \ll 1$. All the motions discussed are two dimensional, taking place in the (r,θ) plane as illustrated.

A. Large Amplitude Waves

To increase one's theoretical understanding of the behavior of low density electron clouds, it is desirable to possess as large a "repertory" of flow solutions as possible. Thus far, the only solutions available have either been steady flows, or small amplitude perturbations of these steady flows. We can now exhibit a new class of large amplitude, unsteady flows which satisfy the full non-linear equations of motion.

The flows to which we refer have the electrostatic potential given by:

$$\phi = \phi_0 \left[\frac{r^2}{a^2} + a_0 J_0(kr) + a_\ell J_\ell(kr) \sin(\ell\theta - \omega t) \right] \qquad (5a.1)$$

ϕ_0 is a constant reference potential, J_ℓ is the Bessel function of order ℓ, a_0 and a_ℓ are the arbitrary constants, k is any one of the roots of the equation

$$J_\ell(ka) = 0 \qquad (5a.2)$$

and the frequency ω is given by

$$\frac{\omega}{\ell} = \frac{2\phi_0}{Ba^2} = \frac{n_0 e}{2\epsilon_0 B} = \frac{\omega_0}{2} = \frac{1}{2}\frac{\omega_p^2}{\omega_c} \qquad (5a.3)$$

n_0 is a reference electron number density, ℓ (an integer ≥ 1) is a mode

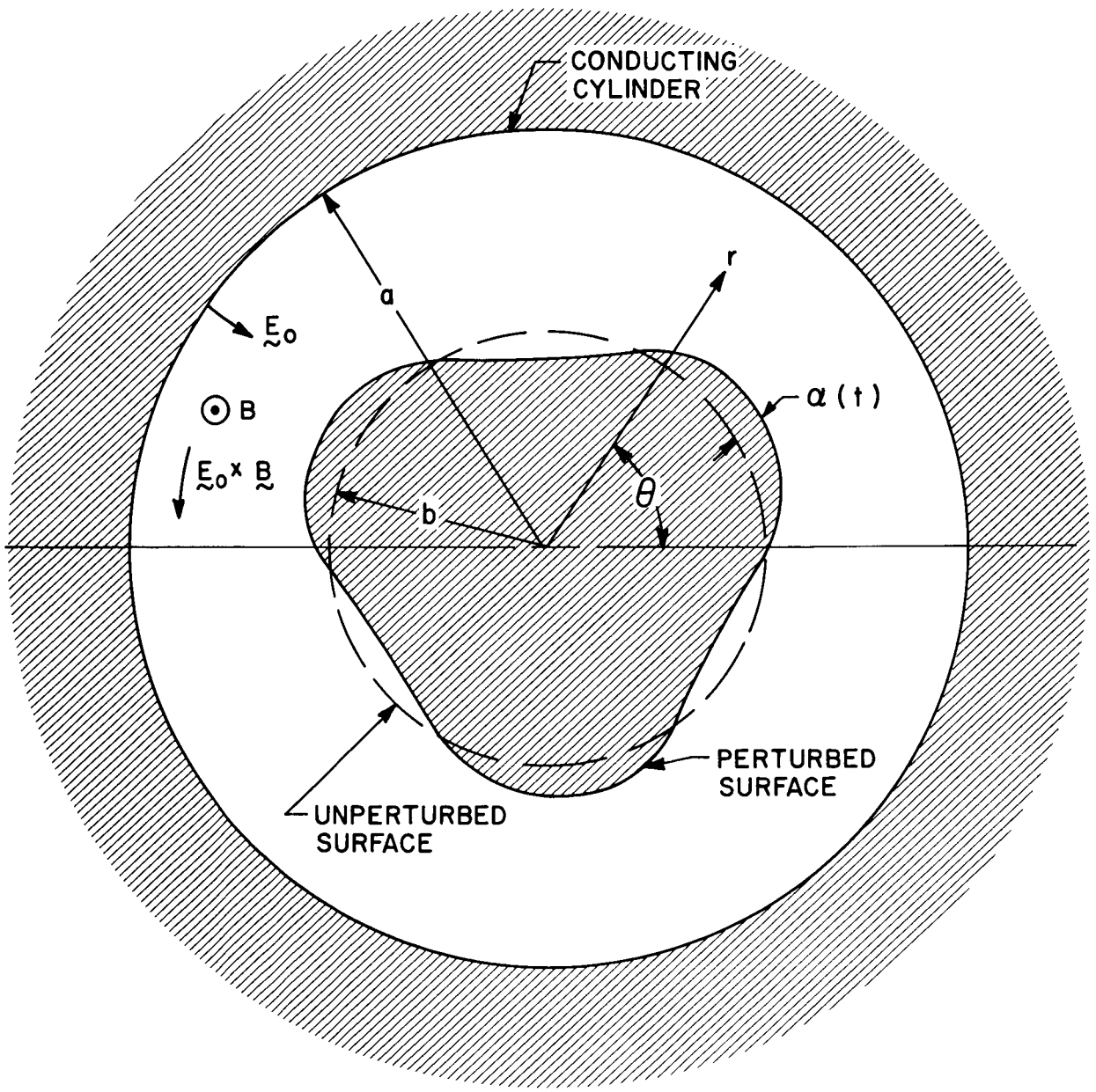

Fig. V-1 Basic geometry for theoretical studies. An infinite conducting cylinder of radius a contains a uniform magnetic field B in the z direction. This figure also shows a representation of a diocotron wave as a perturbation of the surface of the electron cloud. An $\ell = 3$ wave is shown. The unperturbed (wave free) state is the circle of radius b. The wave perturbation is given by the small periodic radial displacement of the surface α.

number.

To prove that (5a.1) represents a satisfactory solution for the space-charge flow, we observe first that it is zero (and regular) when $r = 0$, and that

$$\phi(a,\theta,t) = \phi_0 [1 + \alpha_0 J_0(ka)] = \text{constant} \qquad (5a.4)$$

Thus the boundary condition that ϕ be constant on the conducting cylinder $r = a$ is satisfied.

Next, we derive the radial and tangential electric fields. These are:

$$E_r = -\frac{\phi_0}{a}\left[\frac{2r}{a} + \alpha_0 ka\, J_0'(kr) + \alpha_\ell ka\, J_\ell'(kr)\sin(\ell\theta - \omega t)\right]$$

$$E_\theta = -\frac{\phi_0}{a}\left[\frac{a}{r}\,\ell\,\alpha_\ell J_\ell(kr)\cos(\ell\theta - \omega t)\right] \qquad (5a.5)$$

The radial and tangential velocities u_r, u_θ follow from E_r, E_θ according to:

$$\underset{\sim}{E} + \underset{\sim}{u} \times \underset{\sim}{B} = 0 \qquad (5a.6)$$

or:

$$u_r = \frac{E_\theta}{B} \qquad u_\theta = -\frac{E_r}{B} \qquad (5a.7)$$

To find the electron density n, we take the divergence of (5a.5)

$$n = -\frac{\epsilon_0}{e}\left[\frac{1}{r}\frac{\partial}{\partial r}(rE_r) + \frac{1}{r}\frac{\partial E_\theta}{\partial\theta}\right]$$

$$= n_0\left[1 - \frac{\alpha_0}{4}(ka)^2 J_0(kr) - \frac{\alpha\ell}{4}(ka)^2 J_\ell(kr)\sin(\ell\theta - \omega t)\right] \qquad (5a.8)$$

The last step in showing that our solution is satisfactory is the demonstration that the equation of continuity:

$$\frac{\partial n}{\partial t} + \frac{1}{r} \frac{\partial}{\partial r} (n u_r r) + \frac{1}{r} \frac{\partial}{\partial \theta} (n u_\theta) = 0 \qquad (5a.9)$$

is satisfied. Using the fact that curl $\underset{\sim}{E} = 0$, the continuity equation simplifies to

$$\frac{\partial n}{\partial t} + u_r \frac{\partial n}{\partial r} + \frac{u_\theta}{r} \frac{\partial n}{\partial \theta} = 0 \quad . \qquad (5a.10)$$

Remembering that the frequency ω is given by (5a. 3) it is easily shown by direct substitution that this equation is satisfied.

In considering the meaning of these solutions it is convenient to think of the form (5a. 1) as representing a steady-state, with a superposed wave-like term proportional to $\sin(\ell\theta - \omega t)$. For example, integrating the number density n across the surface of the cylinder, the wave-like term will give no contribution. Thus, the mean number density $\bar{n}$ is:

$$\bar{n} = n_0 \left[1 - \frac{a_0}{2} \int_0^{ka} x J_0(x)\, dx \right] = n_0 \left[1 - \frac{a_0}{2} ka J_1(ka) \right] \qquad (5a.11)$$

The solution exhibited above (Eq. (5a. 8) contains two arbitrary constants a_0 and a_ℓ in addition to the mode number ℓ. The only condition on the a's is that the density should be nowhere negative. Of course, if a_ℓ is very small, the solution is precisely the one that would be obtained by making a small (linear) perturbation about the steady part of the solution.

To exhibit some typical cases of this solution we first set $\ell = 1$, and take ka equal to the first zero of J_1. Thus:

$$ka = 3 \cdot 832 \ldots \qquad (5a.12)$$

Notice that in the case $\ell = 1$, from (5a. 11), since $J_1(ka) = 0$,

$$\bar{n} = n_0 \quad . \qquad (5a.13)$$

Shown in Fig. V-2 are "unperturbed" density profiles for two values of a_0. First

$$a_0 = \frac{4}{(ka)^2 J_0(ka)} = -.6763 \qquad (5a.14)$$

for which the unperturbed density is

$$\frac{n}{n_0} = 1 - \frac{J_0(kr)}{J_0(ka)} \qquad (5a.15)$$

For this value of a_0, n/n_0 (unperturbed) = 0 when $r = a$. The second value of a_0 is

$$a_0 = \frac{4}{(ka)^2} = .2724 \qquad (5a.16)$$

for which the unperturbed density is

$$\frac{n}{n_0} = 1 - J_0(kr) \quad . \qquad (5a.17)$$

For this value of a_0, n/n_0 (unperturbed) = 0 when $r = 0$. In Fig. V-3 are shown contours of the perturbed density

$$\frac{n}{n_0} = a_1 J_1(kr) \sin(\theta - \omega t) \quad . \qquad (5a.18)$$

B. Small Amplitude Fundamental Diocotron Waves

When $\ell = 1$ (fundamental mode), by using Eq. (5a.13) we find that the total charge per unit length in the exact non-linearized solution of the previous section is just

$$Q = \pi a^2 \bar{n} e = \pi a^2 n_0 e \quad . \qquad (5b.1)$$

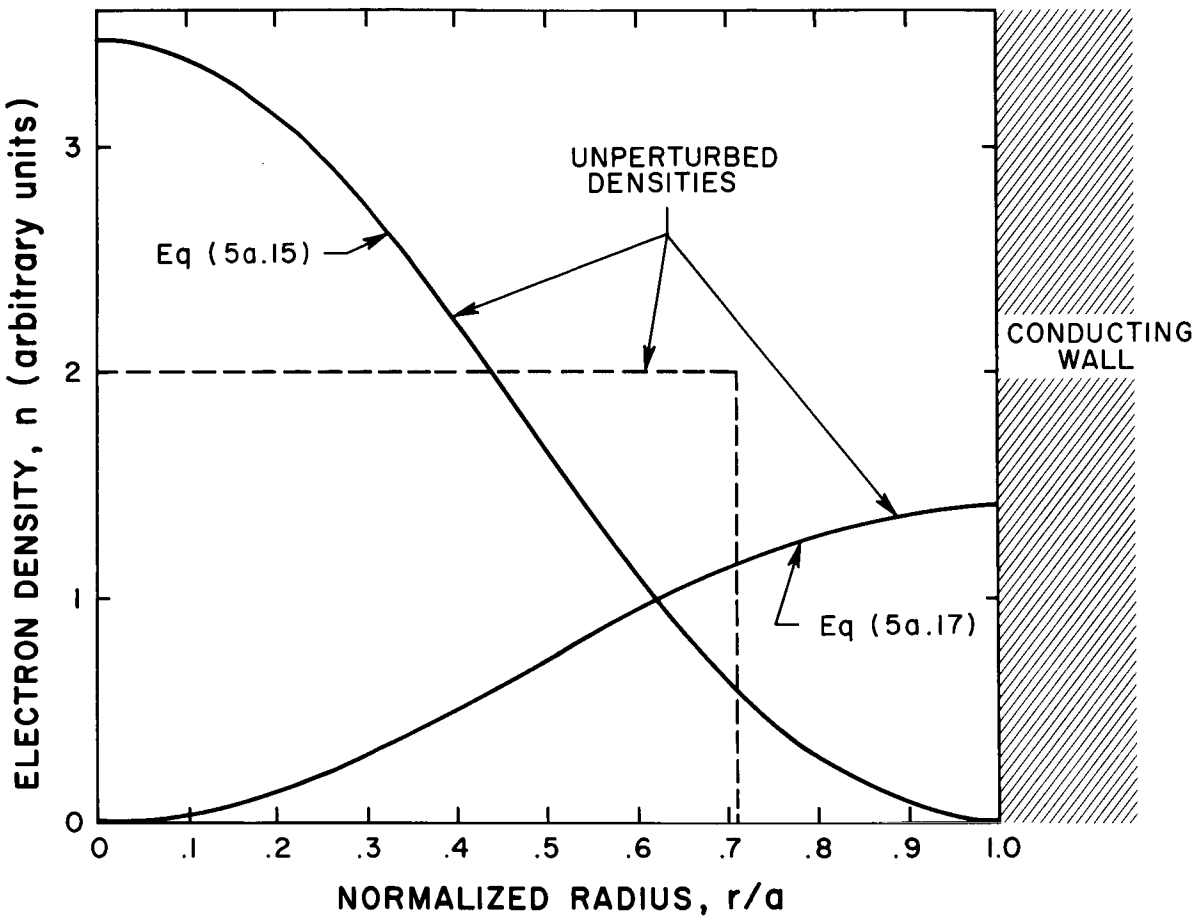

Fig. V-2 The solid curves show typical unperturbed electron densities as given by equations (5a.15) and (5a.17) of the text. These densities are shown in the text to support analytically calculable non-linear wave solutions. The dashed curve shows a typical uniform density used for linearized wave solutions.

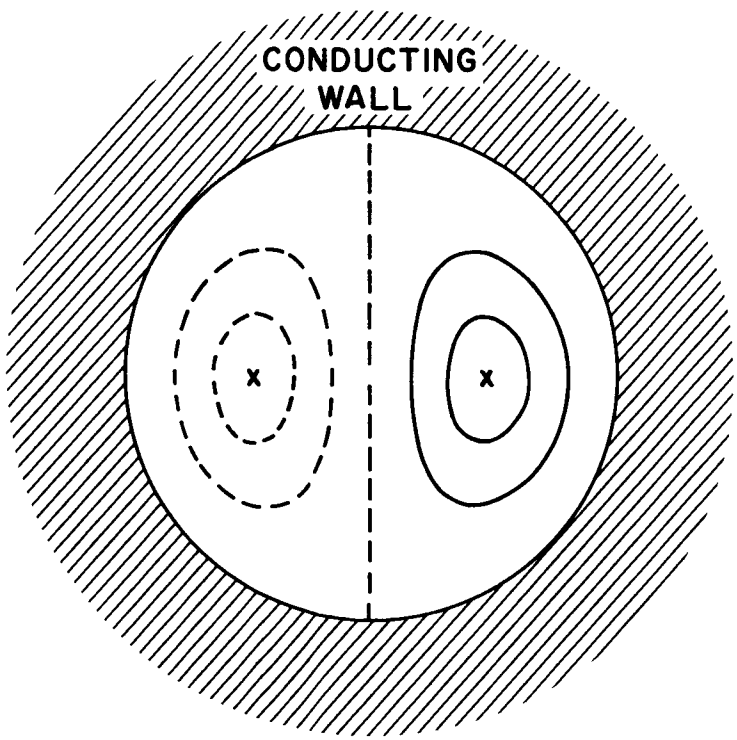

Fig. V-3 Equipotentials of the non-linear wave, equation (5a.18). The mode shown is the dipole oscillation mode ($\ell = 1$). The solid lines represent equipotentials of one sign of the oscillation (say, $\phi_1 > 0$) while the dashed represent the other sign (say, $\phi_1 < 0$).

Hence, it follows that the frequency of the mode is

$$\omega = \frac{Q}{2\pi a^2 \epsilon_0 B} \tag{5b.2}$$

Linear analysis of the unperturbed density distribution:

$$\left.\begin{aligned} n &= n_0 \qquad (0 \leq r \leq \lambda a) \\ n &= 0 \qquad (\lambda a \leq r \leq a) \end{aligned}\right\} \quad (\lambda < 1) \tag{5b.3}$$

yields a frequency for the fundamental mode

$$\omega = \frac{n_0 e}{2\epsilon_0 B} \lambda^2 \ . \tag{5b.4}$$

But in this case,

$$Q = \pi a^2 n_0 e \lambda^2 \tag{5b.5}$$

so that again

$$\omega = \frac{Q}{2\pi a^2 \epsilon_0 B} \ , \tag{5b.6}$$

i.e., the same frequency as in (5b.2) above. In the current experiments (Section 6a) the frequency of the fundamental diocotron mode is measured by the current buttons. If the "unperturbed" density distribution is that of either of the two cases above, the frequency measured in the laboratory would allow the direct estimation of the total charge in experiment. It would be of great value if it could be shown that the frequency of the fundamental mode was a measure only of the charge, no matter what the distribution of electron density with radius. It has been possible to prove this assertion precisely for small amplitude waves.

If the unperturbed density distribution is an arbitrary function $n_0(r)$,

the potential of a diocotron disturbance in the fundamental mode has the form $\phi(r)\, e^{i(\theta - \omega t)}$. Then, using Poisson's equation, the equation of continuity yields the following equation governing the small quantity $\phi(r)$:

$$\left(r\omega + \frac{E_0}{B}\right)\left\{\frac{1}{r}\frac{d}{dr}\left(r\frac{d\phi}{dr}\right) - \frac{\phi}{r^2}\right\} = \phi\left\{\frac{1}{r}\frac{d}{dr}\left(r\frac{dE_0/B}{dr}\right) - \frac{E_0/B}{r^2}\right\} \tag{5b.7}$$

E_0 is the unperturbed radial electric field. It is very simple to show that the right hand side of (5b.7) can without change be re-written as:

$$\phi\left\{\frac{1}{r}\frac{d}{dr}\left\{r\frac{d}{dr}\left(r\omega + \frac{E_0}{B}\right) - \frac{(r\omega + E_0/B)}{r^2}\right\}\right\} \tag{5b.8}$$

and it follows by inspection that a solution of this equation is

$$\phi = \text{const} \times [r\omega + E_0/B] \,. \tag{5b.9}$$

Where one solution of a differential equation of this type is known, the other can always be simply derived. It is:

$$\phi = \text{const} \times \left(r\omega + \frac{E_0}{B}\right)\int \frac{dr}{r[r\omega + E_0/B]^2} \tag{5b.10}$$

These two solutions together with the trivial solution $\phi = 0$ represent all possible solutions to the differential equation (5b.7). As we shall discuss below, there are critical points ($r = r_{critical}$) of the differential equation on either side of which different linear combinations of the solutions (5b.9) and (5b.10) or the trivial solution $\Phi \equiv 0$ can be chosen in order to satisfy the appropriate boundary conditions. For reasonable density distributions the solution (5b.9) behaves like r near $r = 0$, and the solution (5b.10) behaves like r^{-1} near $r = 0$. Therefore, for $0 \leq r \leq r_{critical}$ we must choose the solution (5b.9).

Now first we should observe that Eq. (5b.9) is a satisfactory solution for all r, and is itself therefore a possible eigenfunction. The

frequency ω for this eigenfunction is determined by the boundary condition $\Phi(a) = 0$, so that

$$\omega = - \frac{E_0(a)}{aB} \tag{5b.11}$$

However, from Gauss' theorem,

$$E_0(a) = - \frac{Q}{2\pi \epsilon_0 a} \tag{5b.12}$$

so that again we find

$$\omega = \frac{Q}{2\pi \epsilon_0 a^2 B} \tag{5b.13}$$

in agreement with our assertion that the frequency of the fundamental mode is a measure of the total charge per unit length, independent of its distribution in radius.

This result, useful in itself, shows that there is a fundamental mode having the desired property. However, it would be a much more useful result if it could be shown that it was the only fundamental mode. We shall now show that, while it is not the only fundamental mode, it is, however, the only fundamental mode which can be measured by the current buttons.

Both sides of (5b.7) can vanish at certain special points; i.e., the critical points previously mentioned. The left-hand side can vanish at any place r^*, provided

$$\omega = - \frac{E_0(r^*)}{r^* B} \tag{5b.14}$$

Also, if ϕ is given by (5b.9), the left-hand side will vanish for any ω at points for which

$$\frac{1}{r} \frac{d}{dr} \left(r \frac{dE_0}{dr} \right) - \frac{E_0}{r^2} = \frac{d}{dr} \left\{ \frac{1}{r} \frac{d}{dr} (rE_0) \right\} = - \frac{e}{\epsilon_0} \frac{dn_0}{dr} = 0 \tag{5b.15}$$

Such special points occur whenever n_0 has a maximum or minimum. The right-hand side of (5b. 7) can vanish when $\phi = 0$, or at maxima or minima of n_0.

Let us consider first the situation in which ω is given by (5b. 14). Then $\phi(r^*) = 0$, since for $0 \le r \le r^*$ ϕ is given by (5b. 9). For $r^* \le r \le a$ ϕ may be of a different form, provided only that ϕ and ϕ' are continuous at $r = r^*$. Suppose ϕ is given for $r^* \le r \le a$ by

$$\phi = \text{const} \left(r\omega + \frac{E_0}{B} \right) \int_r^a \frac{dr}{r\left(r\omega + \frac{E_0}{B} \right)^2} \qquad (5b.16)$$

The upper limit in the integral must be a since $\phi(a) = 0$. But for ϕ to be continuous at $r = r^*$, $\phi(r^*)$ must also be zero, or

$$\left(r^*\omega + \frac{E_0(r^*)}{B} \right) \int_{r^*}^a \frac{dr}{r(r\omega + E_0/B)^2} = 0 \qquad (5b.17)$$

Since the function $[\, r\omega + E_0(r)/B \,]$ is known to vanish at $r = r^*$, this integral is singular. Now near $r = r^*$,

$$\left(r\omega + \frac{E_0}{B} \right) = (r - r^*) \left[\omega + \frac{E_0'(r^*)}{B} \right] + \frac{1}{2} (r - r^*)^2 \frac{E_0''(r^*)}{B} + \ldots \qquad (5b.18)$$

If $\omega + \dfrac{E_0'(r^*)}{B} \neq 0$, the expression on the left of (5b. 17) reduces to

$$\frac{1}{r^* \left[\omega + \dfrac{E_0'(r^*)}{B} \right]} \qquad (5b.19)$$

which can never by zero. If $\omega + \dfrac{E_0'(r^*)}{B}$ is zero, the situation is even

worse, the expression on the left of (5b.17) being singular. The only remaining alternative is that for $r^* \leq r \leq a$,

$$\phi \equiv 0 \quad . \tag{5b.20}$$

This solution ensures that ϕ is continuous at $r = r^*$; we also require that ϕ' be continuous, which ovbiously means that $\phi'(r^*) = 0$. This condition is satisfied only if

$$\omega + \frac{E_0'(r^*)}{B} = 0 \tag{5b.21}$$

Thus we have found a number of additional modes of oscillation. If there is any point $r = r^*$ such that

$$\frac{E_0(r^*)}{r^*} = E_0'(r^*) \quad , \tag{5b.22}$$

then there is a mode of oscillation with the frequency

$$\omega = - \frac{E_0(r^*)}{r^* B} \tag{5b.23}$$

However, for all such modes we have shown $\phi \equiv 0$ for $r^* \leq r \leq a$, and hence the mode has no radial electric field $\phi'(a)$ at the wall. Therefore, the mode can not be detected by current buttons, which measure $\phi'(a)$.

The remaining possibility is that there is a mode associated with an extremum of n_0. At such a point (5b.7) is satisfied whatever the value of ϕ . Tnus, for $0 \leq r \leq r^*$

$$\phi = r\,\omega + \frac{E_0}{B} \tag{5b.24}$$

and for $r^* \leq r \leq a$

$$\phi = \left[r\omega + \frac{E_0}{B} \right] \int_r^a \frac{dr}{r\left[r\omega + \frac{E_0}{B} \right]^2} \qquad (5b.25)$$

ω is not yet determined. The continuity of ϕ requires that

$$\int_{r^*}^a \frac{dr}{r\left[r\omega + \frac{E_0}{B} \right]^2} = 1 \quad , \qquad (5b.26)$$

which is an equation for ω. However, in addition to the continuity of ϕ we require ϕ' to be continuous. This turns out to be:

$$\frac{1}{r^*\left[r^*\omega + E_0(r^*)/B \right]} = 0 \qquad (5b.27)$$

As this condition is impossible, we conclude that there are no modes for which $\phi'(a) \neq 0$, except the one with which we started, and that the frequency of this mode measures the total charge per unit of length independent of its distribution. This result is of great value in interpreting experimental frequency measurements. Note, however, that, for a given total charge, the potential is dependent on the way in which the charge is distributed. Thus it is not possible to calculate the potential from the frequency of the fundamental mode without further measurements, or assumptions.

C. Adiabatic Compression of the Diocotron Wave

We have established in the previous section that the frequency of the fundamental mode measured by current buttons provides a valuable diagnostic tool for determining the total charge contained in the device. Before one can obtain quantitative information from the measured amplitude of these oscillations it is necessary to understand how the amplitude of these oscillations changes as the charge distribution is compressed during the slow increase in magnetic field.

In a cylinder of radius a, the unperturbed density n_0 is taken to be constant to a radius b. The diocotron oscillation of mode number ℓ represents a displacement Δ of the surface in the form

$$\Delta(\theta, t) = a(t) \sin(\ell\theta - \omega t) \; ; \quad a(t) \ll b(t) \qquad (5c.1)$$

where the amplitude of the oscillation a as well as the radius of the edge of the cloud $b(t)$ are functions of time due to the changing magnetic field (see Fig. V-1). The dependence of a on time is correctly given in the case of the fundamental ($\ell=1$) mode by a simple argument based upon the motion of the center of charge. If the electron cloud is allowed to shrink to zero radius, the perturbation (5c.1) represents a displacement of the resulting line charge a distance a from the axis of the conducting cylinder. For small a, the electric field produced by the induced image charge causes a rotation with the correct diocotron frequency given by (5b.13). As the line charge rotates the flux it encircles is $B(t)\,\pi\,a(t)^2$. As long as $\dot{B}/B\omega \ll 1$, the above quantity is the third adiabatic invariant which is conserved as $B(t)$ changes. We thus obtain the correct small amplitude result,

$$a(t) \propto B(t)^{-1/2} \qquad (5c.2)$$

for the displacement as a function of time.

We shall now show that the above result is valid for any mode ℓ and in the case of only one free surface with which we are here concerned the result is exact rather than an adiabatic. The equation for the surface can be written

$$F(r, \theta, t) \equiv b(t) + a(t) \sin(\ell\theta - \omega t) - r = 0 . \qquad (5c.3)$$

The motion of the free surface can be obtained from the continuity equation

$$\frac{DF}{Dt} \equiv \frac{\partial F}{\partial t} + V_r \frac{\partial F}{\partial r} + V_\theta \frac{1}{r} \frac{\partial F}{\partial \theta} = 0 ,$$

where the velocity is to be evaluated at the edge of the cloud. With B in the positive Z-direction and using $\underline{V} = E\,B/B^2$, we readily obtain

$$\dot{b}(t) - \frac{E_\theta}{B(t)} + \dot{a}(t) \sin(\ell\theta - \omega t) - \left(\omega + \frac{\ell E_r}{Br}\right) a(t) \cos(\ell\theta - \omega t) = 0 . \qquad (5c.4)$$

We shall satisfy this equation for small amplitude waves, i.e., to first

order in the perturbation a . The zero'th order expression $E_r = -\frac{en_0 b}{2\epsilon_0}$ can be used for the radial electric field; however E_θ must be evaluated carefully through first order in a . The equation $\nabla \times E = -\dot{B}$ yields

$$E_\theta = \left(-\frac{1}{2} Br - \frac{1}{r}\frac{\partial \phi(r)}{\partial \theta}\right) \sin(\ell\theta - \omega t)\Big|_{r = b + a\sin(\ell\theta - \omega t)}$$

$$= -\frac{1}{2} B\left[b(t) + a(t)\sin(\ell\theta - \omega t)\right] - \frac{\ell}{b}\phi(b)\cos(\ell\theta - \omega t) \qquad (5c.5)$$

where $\phi(r)$ is the solution of Poisson's equation for the perturbed potential:

$$\phi(r) = -\frac{en_0}{2\epsilon_0 \ell b^{\ell-1}}\left[1 - \left(\frac{b}{a}\right)^{2\ell}\right] r^\ell \; ; \qquad r \le b$$

$$\phi(r) = -\frac{en_0 b^{\ell+1}}{2\epsilon_0 \ell a^\ell}\left[\left(\frac{a}{r}\right)^\ell - \left(\frac{r}{a}\right)^\ell\right] ; \qquad b \le r \le a \; . \qquad (5c.6)$$

Equations (5c.6) are most easily obtained by treating the quantity $-en_0 a(t)\sin(\ell\theta - \omega t)$ as a surface charge density concentrated at the unperturbed radius $b(t)$. Substituting $\phi(b)$ into Eq. (5c.5) and combining with Eq. (5c.4) allows one to obtain the frequency of oscillation

$$\omega = \frac{\ell}{bB}\left[-E_r + \phi(b)/a\right] = \frac{en_0}{2\epsilon_0 B}\left[\ell - 1 + \left(\frac{b}{a}\right)^{2\ell}\right] \qquad (5c.7)$$

from the cosine term. The secular term integrates to give $b(t) \propto B(t)^{-1/2}$ which expresses the conservation of flux. This result together with the conservation of charge yields the previously known result that

$$\frac{n_0}{B} = \text{constant.}$$

The coefficient of the sin term is easily integrated to yield Eq. (5c. 2) which expresses the time behavior of the amplitude of any mode of oscillation. In addition, we see that it is an exact result of the linear analysis and is hence valid for any value of $\dot{B}$ rather than only valid adiabatically for slow changes in the magnetic field.

It is often stated that the action $A \equiv \mathcal{E}/\omega$, where $\mathcal{E}$ is the total energy of the wave, is conserved for slow changes. We now show that when the total energy of the wave (the sum of a frame independent electrostatic contribution and a frame dependent electrostatic contribution due to displacement of the electrons in the zeroth order electrostatic potential) is employed, the result (5c. 2) guarantees that action is indeed conserved. The frame independent electrostatic energy per unit axial length of the wave is

$$\mathcal{E}_{el} = \frac{\epsilon_0}{2} \int_0^a \left[\phi'(r)^2 + \frac{\ell^2}{r^2}\,\phi(r)^2\right] \pi\, r\, dr = -\frac{1}{2}\, en_0\, a\, \pi b \phi(b) \quad . \qquad (5c. 8)$$

Working in the laboratory frame, the change in energy of the wave electrons due to their displacement in the zeroth order electrostatic field is given by

$$\mathcal{E}_p = -\iint (-en_1)\,\frac{\overline{\Delta}}{2} \cdot \overline{E}\; r\, dr\, d\theta = \frac{1}{2}\int_0^{2\pi}\int_0^a en_0\, a^2 \sin^2(\ell\theta - \omega t)\,\delta(r-b) E_r\, r\, dr\, d\theta$$

$$= \frac{1}{2}\, en_0\, \pi a^2 b\, E_r \quad . \qquad (5c. 9)$$

In Eq. (5c. 9) the average displacement $\Delta/2$ of the charge density en_1 is used. This result is dependent on the frame of reference as the radial electric field depends on the frame. Combining (5c. 6) with (5c. 8) and (5c. 9) and using (5c. 7), we readily obtain for the action per unit length

$$A = \frac{\mathcal{E}_{el} + \mathcal{E}_p}{\omega} = \frac{en_0\, \pi a b}{2\omega}\,[a E_r - \phi(b)] = -\frac{en_0 \pi a^2 b^2 B}{2\ell} = -\frac{Q\, a^2 B}{2\ell} \quad .$$

Thus $a \propto B^{-1/2}$ is consistent with the conservation of action during the change in magnetic field.

In order to make use of this result as a diagnostic, it is necessary to know how the perturbed fields affect the signal picked up by the current

buttons. The electric field at the wall is obtained from Eq. (5c.6):

$$E_r = -\frac{\partial}{\partial r} = \frac{en_0}{\epsilon_0}\left(\frac{b}{a}\right)^{\ell+1} \propto B^{-\frac{\ell}{2}}$$

and is proportional to the induced surface charge at the wall. Generally, the signal measured is the image current which is proportional to ωE_r or

$$i_{measured} \propto \omega E_r \propto B^{-\frac{\ell}{2}}\left[\ell - 1 + \left(\frac{b}{a}\right)^{2\ell}\right] \propto \begin{cases} B^{-3/2} & \ell = 1 \\ B^{-\frac{\ell}{2}} & \ell \geq 2;\ b \ll a\,. \end{cases}$$

We have seen that with one discontinuous surface the amplitude of a surface wave varies as $B(t)^{-1/2}$ which is an exact result. The situation changes when there are two discontinuous surfaces each of which supports a surface wave. The equation describing the time dependence of the perturbation amplitude is now second order and hence cannot be integrated exactly. However, when the unperturbed configuration is stable (and far from the conditions for marginal stability), WKB solutions can be used to obtain precisely the expected result given by Eq. (5c.2). This result is now only an approximation and is valid adiabatically for small $\dot{B}$. Its validity depends not only on the rate of change of magnetic field, but also on the system not being near the unstable configuration. In this adiabatic sense, the conservation of action provides a simple principle for giving the variation of perturbation amplitude with magnetic field for more complicated geometrical situations.

VI. Experimental Results

A. Diocotron Wave Diagnostics

During this quarter it was empirically observed and subsequently confirmed theoretically that the frequency of the fundamental mode of diocotron wave oscillation (i.e., the $\ell = 1$ or dipole mode) is uniquely related to the total charge in the system. These signals were observed on image current buttons located at the top and bottom of the torus as shown on Fig. VI-1. Fig. VI-2 shows a typical oscilloscope trace observed using these buttons. As in this figure, the frequency measurement is usually at a time shortly after crowbarring the magnetic field -- that is, when the magnetic field is essentially constant. However, this is not a restriction since by recording the magnetic field, frequency measurements taken at any time can be interpreted. Knowing the frequency and the magnetic field one can calculate the total charge from Eq. (5b. 13), which for our present apparatus yields

$$Q \approx 11 \, f \, B \qquad \mu \text{ coulombs} \qquad \text{(6a. 1)}$$

where f is in megacycles and B in webers/m^2. Using this technique the maximum injected charge to date has been measured at about 40 μ coulombs.

B. Electrostatic Potential

As indicated in previous progress reports, the electrostatic voltage probe is useful below voltages of the order of 100 kv. However, by using the diocotron wave frequency and integrated current button (see Quarterly Progress Report NAS8-20310, March 1967) techniques to measure the charge in the system and then by cross correlating these measurements with voltage probe measurements at low electrostatic potentials, we have been able to infer the existence of a well depth in excess of 200 kv for a maximum injected charge of 40 μ coulombs.

Fig. VI-1 shows the method used for extrapolation of voltage probe measurements to infer a potential of 200 kv. Probe potentials and charges were measured in the regime of about 5 - 15 μ coulombs. This was accomplished by lowering the capacitor bank voltage and thus both the Φ voltage and the maximum magnetic field. By assuming that the amount of electron cloud compression achieved is essentially constant from experiment to experiment (i.e., the ratio of b/a on Fig. VI-3 is essentially constant for increased Q) we can extrapolate the low voltage probe measurements by using a straight line. The assumption that the compression ratio is constant is probably true and in any case the inferred potentials are only weakly sensitive to changes in the amount of compression (the actual potential varies as a constant plus a logarithm of the compression). Two

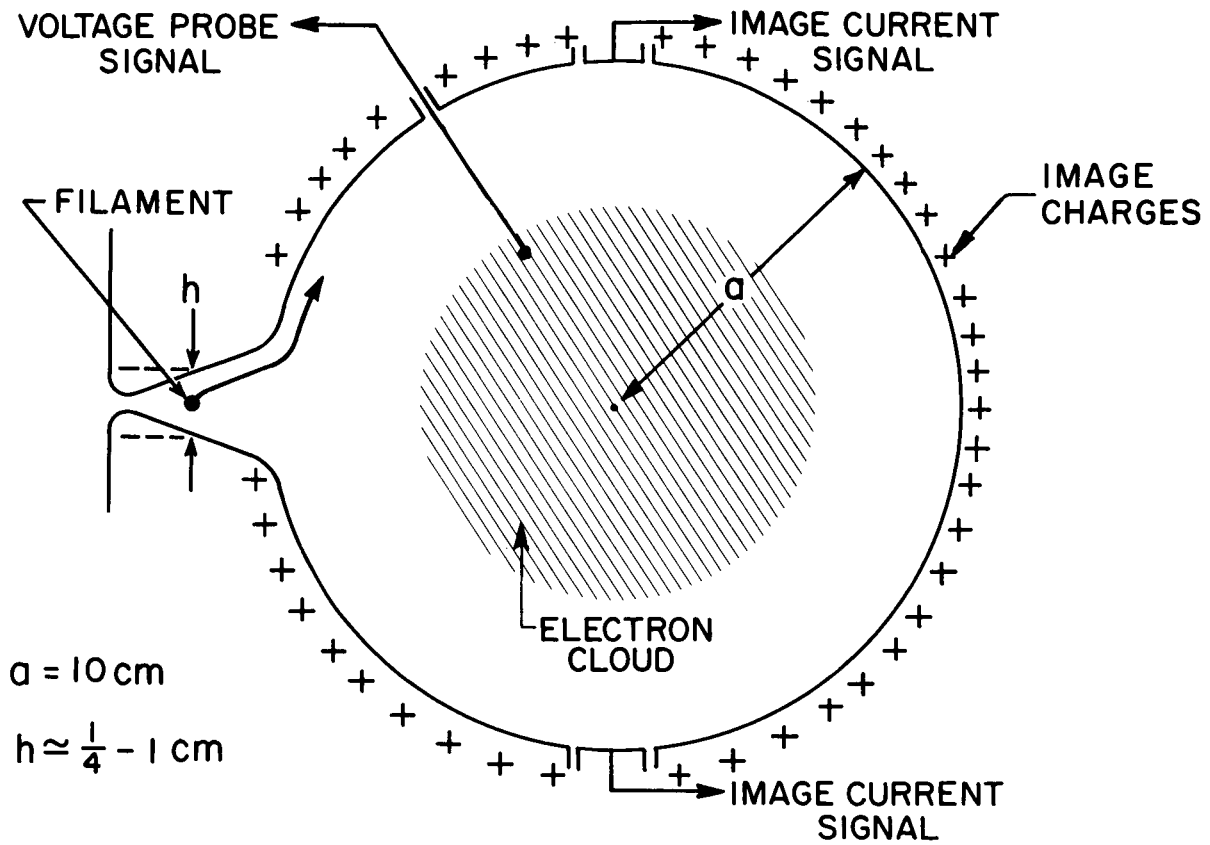

Fig. VI-1 Schematic representation of the present experimental configuration.

A6759X

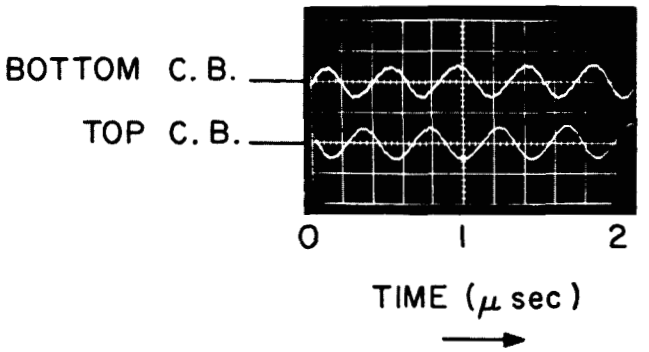

1. PHASE LAG INDICATES FUNDAMENTAL MODE
2. TIME OF OBSERVATION IS 3μ sec AFTER CROWBARRING AT MAX. B.
3. TOTAL CHARGE GIVEN BY: Q = 11 f B

Fig. VI-2 Typical current button measurements of the diocotron wave image currents.

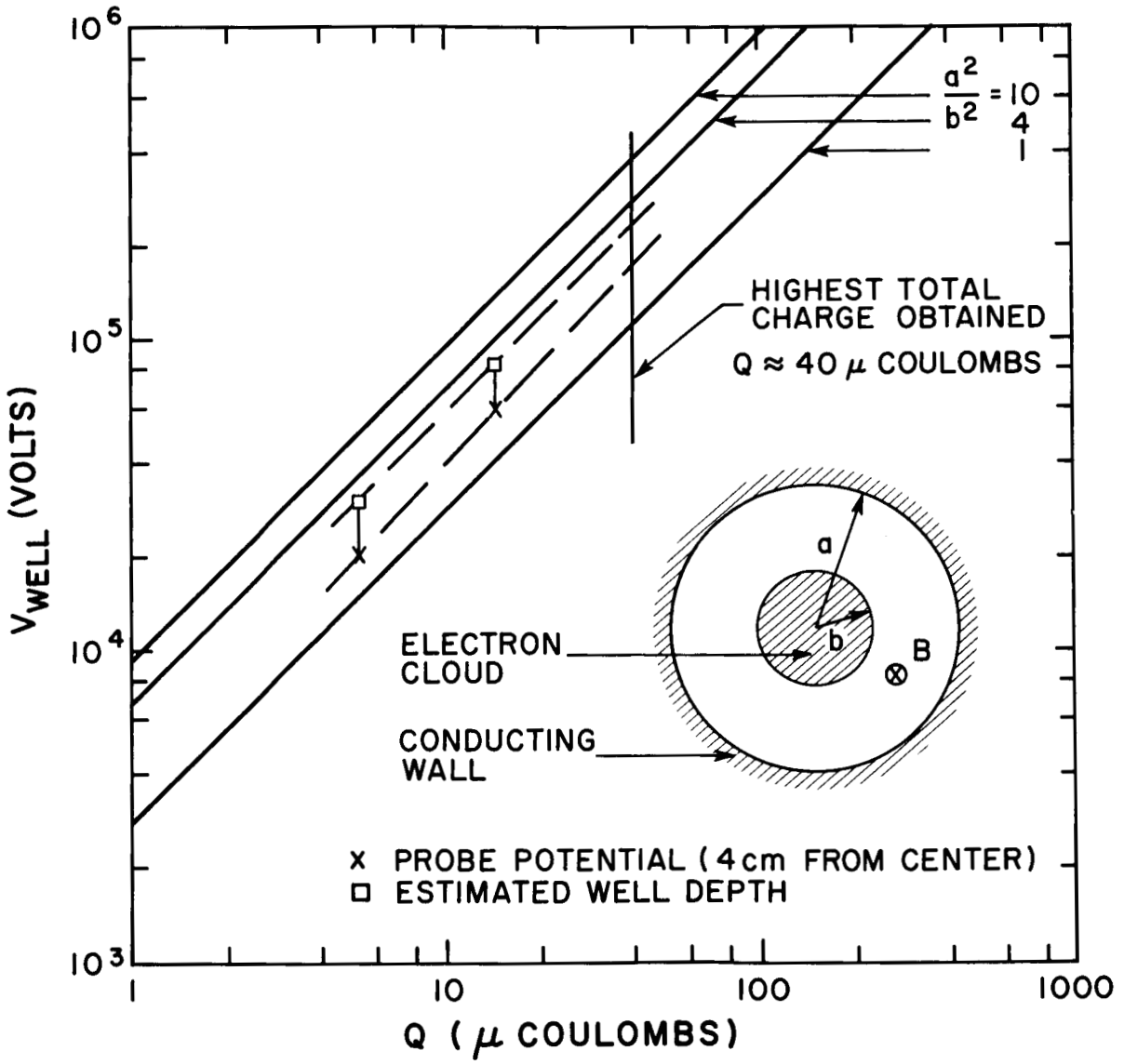

Fig. VI-3 Graphical extrapolation of voltage probe versus injected charge measurements. Linear extrapolation of low voltage (less than 100 kv) measurements indicates that well depths on the axis of the experiment exceeded 200 kv for an injected charge of 40μ coulombs.

probe measurements taken 4 cm off axis are shown of Fig. VI-3. The well depths at the axis plotted on Fig. VI-3 were inferred assuming a uniform distribution of the measured charge. The dashed lines through these points represent our extrapolation and justify the belief that voltages in excess of 200 kv have been achieved.

C. Charge Injection Studies

1) Discussion

During this quarter a major effort has been directed towards defining the various constraining limits which occur during the injection of charge into the torus. One can identify three macroscopic limits which should readily be observed. The first is simply that the well known Hull cut-off must be reached in order to inject charge from the electron launching structure. This implies

$$V_{fil}/B^2 < \text{characteristic constant, say, } N_1 \qquad (6c.1)$$

Since $B \propto \dot{\Phi} t$, this implies that injection does not occur until the Hull cut off time t_H.

The second constraint is that the guiding center drift energy in the large electric fields of the torus must not exceed the electrostatic potential energy of the electron as launched at the filament voltage V_{fil}. This requires

$$e\, V_{fil} \geq \frac{1}{2} m \left(\frac{E}{B}\right)^2_{max} \qquad (6c.2)$$

Certainly this criterion can be qualified by inclusion of a finite magnetic moment; but in general one expects it to exhibit most of the properties of the energy constraint some time after Hull cut-off. Since $E \propto Q$, where Q is the total charge, then by solving equation (6c. 2) for E, we deduce that during injection the current should reach a plateau given by

$$i \propto \sqrt{V_{fil}}\ \dot{\Phi} \qquad (6c.3)$$

The third macroscopic limit has been inferred from experiments reported in the literature on crossed-field amplifiers. In this field,

experimenters have found that when the magnetic field is too large an anomalous amount of noise (i.e., seriously extra-thermal noise) is generated in the crossed-field amplifier. This excess noise, perhaps amplified along the thin electron beam injected into torus, might be expected to cause a breakup of the injection process. Since excess noise has been empirically observed when

$$\frac{V_{fil}}{B^2} < \text{characteristic number, say, } N_2 \qquad (6c.4)$$

and $B \propto \dot{\Phi} t$, we should expect to find a characteristic time during injection beyond which it becomes difficult to inject. From Eq. (6c.4) this characteristic time should vary as

$$t_{critical} \propto \sqrt{\frac{V_{fil}}{\dot{\Phi}}} \qquad (6c.5)$$

2) Experimental Observations

Fig. (VI-4) shows a typical injection current trace observed using a biased current button. One observes the rise in current after about a microsecond. This is Hull cut-off being reached. One then observes that the current reaches a plateau, as suggested by the energy limit discussed above. After about 5 microseconds the current falls off from the plateau. The beginning of this fall-off is interpreted to be the onset of anomalous noise. Subsequent to injection stopping we observe diocotron waves. By measuring their frequency (Section 6.a) we have shown that no charge is lost by these waves during the compression of the cloud (cloud compression takes place from, say, 8 μsec to crowbarring at 37 μsec for Fig. (VI-4)).

On Fig. (VI-4) then, we can observe the injection features discussed in Section (6c. 1) above. To check that the limits on current and critical time are given by the relationships expressed in Eqs. (6c. 3) and (6c. 5), data on maximum current and critical time were taken for a wide range of $\dot{\Phi}$ and V_{fil}. Figs. (VI-5) and (VI-6) plot the results of these measurements.

On Fig. (VI-5) we observe that the data is very well grouped by the correlation and the slope of the data is essentially unity as required. The absolute magnitude of the current is less than one would obtain from Eq. (6c. 2) for a simple cylinder of 10 cm radius by about a factor of 8 to 9. Most of this variation can be accounted for by including the effects of electric field magnification at the transition from the tapered injection

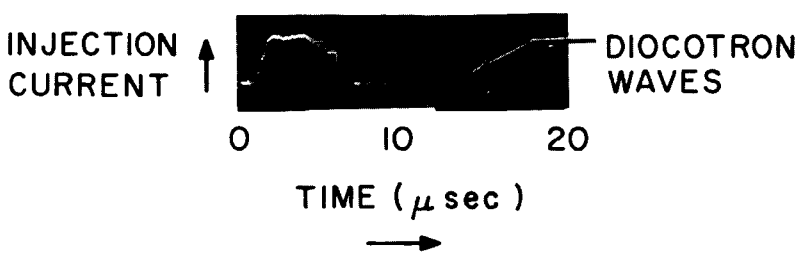

1. MAGNETIC FIELD RISE TIME 37 μ sec.
2. TOTAL CHARGE GIVEN BY $Q = \int I \, dt$

Fig. VI-4 Typical current button image current trace.

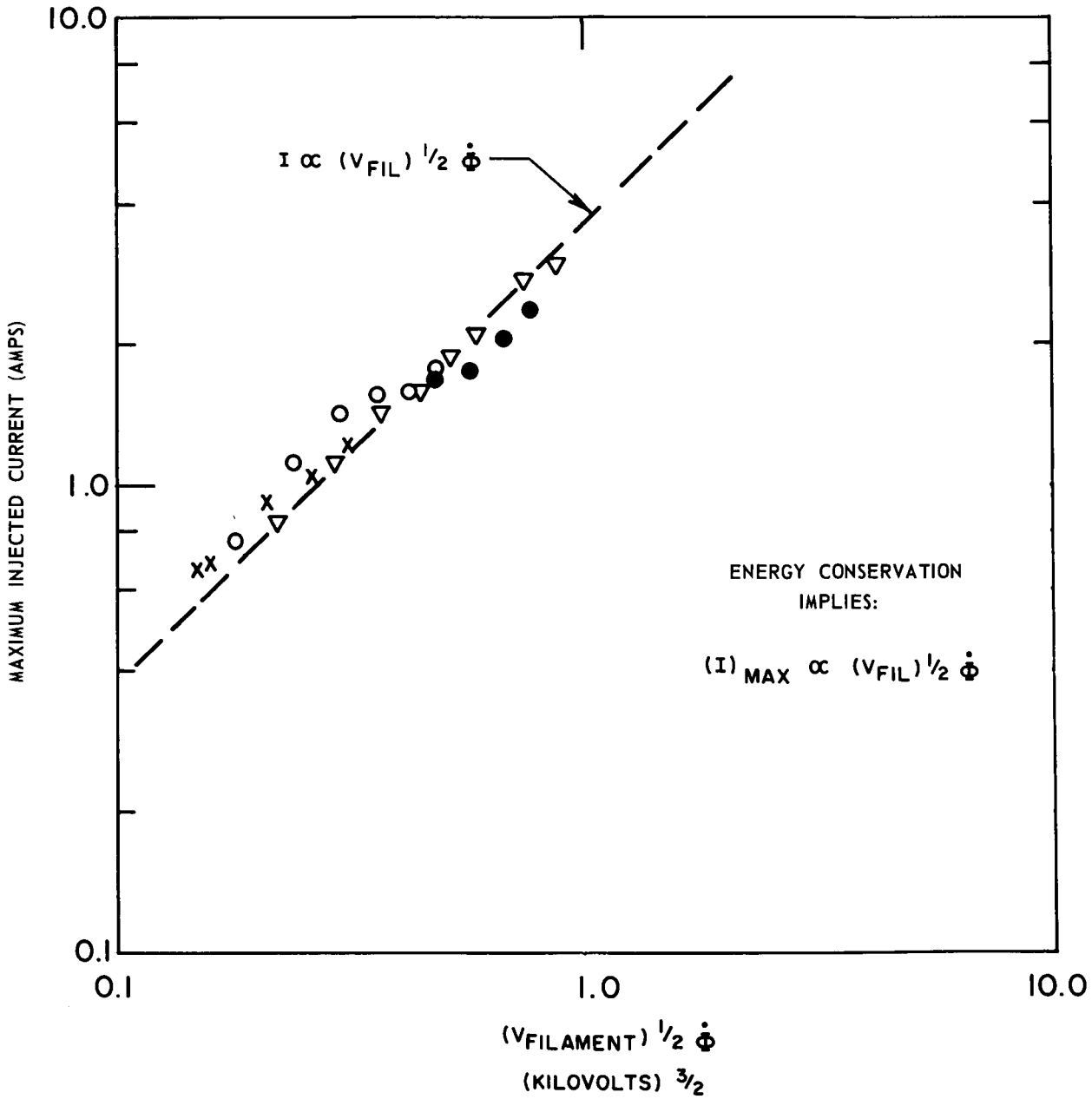

Fig. VI-5 Correlation of the maximum injected current with the quantity $V_{fil}^{1/2}\dot{\Phi}$. The close grouping of the data indicates agreement with the existence of an energy limit as described in the text.

A8263

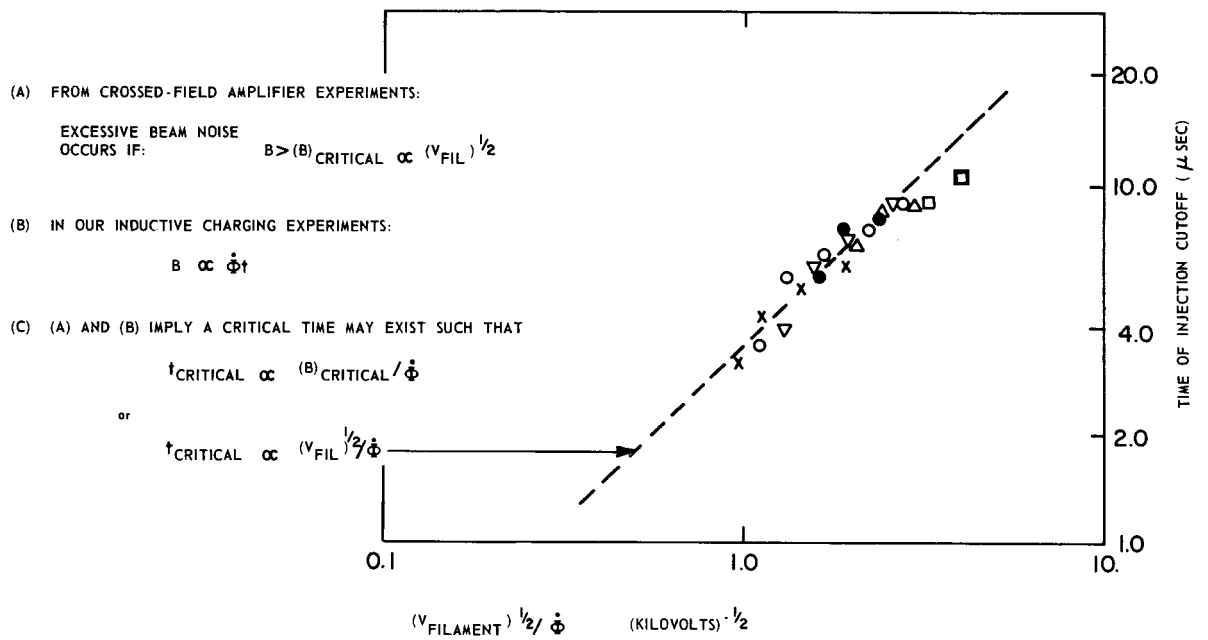

Fig. VI-6 Correlation of $t_{critical}$ with the quantity $V_{fil}^{1/2}/\dot{\Phi}$.

region to the circular torus (see Fig. (VI-1)). The remaining small corrections are likely to be due to the existence of finite amplitude diocotron waves and finite electron magnetic moment. In any case figure (VI-5) shows that the correlation on an energy limit is quite good and suggests that with regard to current injection we are doing as well as possible within the geometrical constraints of the present apparatus.

On Fig. (VI-6) we observe that the data for the critical time measurements is also well grouped by the correlation and has essentially the proper slope. Hence, it seems we can conclude that our present injection is being limited by the occurrence of anomalous noise. To circumvent this limit it will be necessary to program

$$V_f(t) \propto B^2(t) \qquad (6c.6)$$

as a function of time. Using our present correlation, this programming implies a $(V_f)_{max}$ in excess of 100 kv for injecting with magnetic fields of the order of 1 weber/m^2. While not entirely unfeasible, such high voltages are not desirable. Therefore, structural design changes are being considered for the electron launching apparatus which should reduce the voltage required to suppress excess noise.

The results of Figs. (VI-5) and (VI-6) suggest that we should find

$$Q_{injected} \propto V_{fil} \qquad (6c.7)$$

Using the diocotron frequency technique for measuring charge we have confirmed this conclusion over a range of V_{fil} from $0.5\,\dot{\Phi}$ to about $1.5\,\dot{\Phi}$. Below this range, because of electrostatic effects, the filament is back biased and cannot emit. Above the range, electrostatic effects due to the shielding properties of the tapered launching region seem to prevent the full utilization of the filament potential. Experimental changes are being planned for the next quarter to test this hypothesis.

VII. Papers and Presentations

The paper "The Plasma Radiation Shield: Concept, and Applications to Space Vehicles," by Levy and French, will appear as a document of the American Nuclear Society, and also, in shortened form, in the Journal of Spacecraft and Rockets. It is also available as Avco Everett Research Laboratory Research Report 258.

The paper "Computer Experiments on Low Density Crossed-Field Electron Beams," by Levy and Hockney, has now been completed and is available as Avco Everett Research Laboratory Research Report 273. This paper has been submitted for publication to the Physics of Fluids.

The following talks have been given:

1. Invited paper by Levy and French at the meeting of the American Nuclear Society, San Diego, California, entitled "The Status and Prospects for Plasma Radiation Shielding;

2. A short paper by Daugherty, Janes and Levy entitled, "Observations of the Injection, Confinement and Compression of Electron Clouds in a Toroidal Machine," given at the meeting of the American Physical Society, Toronto, Canada;

3. A paper by Daugherty, Eninger, Janes and Levy at the 25th Annual Conference on Electron Device Research, Montreal, Canada, entitled, "Research on the Crossed-Field Injection, Confinement and Compression of Electron Clouds in a Toroidal Machine."